

Structural and Biochemical Characterization of the Type II Fructose-1,6-bisphosphatase GlpX from *Escherichia coli*^{*[S]}

Received for publication, October 25, 2008, and in revised form, December 8, 2008 Published, JBC Papers in Press, December 10, 2008, DOI 10.1074/jbc.M808186200

Greg Brown[‡], Alexander Singer[‡], Vladimir V. Lunin[§], Michael Proudfoot[‡], Tatiana Skarina[‡], Robert Flick[‡], Samvel Kochinyan[‡], Ruslan Sanishvili[¶], Andrzej Joachimiak[¶], Aled M. Edwards[‡], Alexei Savchenko[‡], and Alexander F. Yakunin^{‡1}

From the [‡]Banting and Best Department of Medical Research, University of Toronto, Toronto, Ontario M5G 1L6, Canada, the [§]Chemical and Biosciences Center, National Renewable Energy Laboratory, Golden, Colorado 80401, and the [¶]Biosciences Division, Argonne National Laboratory, Midwest Center for Structural Genomics and Structural Biology Center, Argonne, Illinois 60439

Gluconeogenesis is an important metabolic pathway, which produces glucose from noncarbohydrate precursors such as organic acids, fatty acids, amino acids, or glycerol. Fructose-1,6-bisphosphatase, a key enzyme of gluconeogenesis, is found in all organisms, and five different classes of these enzymes have been identified. Here we demonstrate that *Escherichia coli* has two class II fructose-1,6-bisphosphatases, GlpX and YggF, which show different catalytic properties. We present the first crystal structure of a class II fructose-1,6-bisphosphatase (GlpX) determined in a free state and in the complex with a substrate (fructose 1,6-bisphosphate) or inhibitor (phosphate). The crystal structure of the ligand-free GlpX revealed a compact, globular shape with two α/β -sandwich domains. The core fold of GlpX is structurally similar to that of Li⁺-sensitive phosphatases implying that they have a common evolutionary origin and catalytic mechanism. The structure of the GlpX complex with fructose 1,6-bisphosphate revealed that the active site is located between two domains and accommodates several conserved residues coordinating two metal ions and the substrate. The third metal ion is bound to phosphate 6 of the substrate. Inorganic phosphate strongly inhibited activity of both GlpX and YggF, and the crystal structure of the GlpX complex with phosphate demonstrated that the inhibitor molecule binds to the active site. Alanine replacement mutagenesis of GlpX identified 12 conserved residues important for activity and suggested that Thr⁹⁰ is the primary catalytic residue. Our data provide insight into the molecular mechanisms of the substrate specificity and catalysis of GlpX and other class II fructose-1,6-bisphosphatases.

Fructose-1,6-bisphosphatase (FBPase,² EC 3.1.3.11), a key enzyme of gluconeogenesis, catalyzes the hydrolysis of fructose 1,6-bisphosphate to form fructose 6-phosphate and orthophosphate. It is the reverse of the reaction catalyzed by phosphofructokinase in glycolysis, and the product, fructose 6-phosphate, is an important precursor in various biosynthetic pathways (1). In all organisms, gluconeogenesis is an important metabolic pathway that allows the cells to synthesize glucose from noncarbohydrate precursors, such as organic acids, amino acids, and glycerol. FBPases are members of the large superfamily of lithium-sensitive phosphatases, which includes three families of inositol phosphatases and FBPases (the phosphoesterase clan CL0171, 3167 sequences, Pfam data base). These enzymes show metal-dependent and lithium-sensitive phosphomonoesterase activity and include inositol polyphosphate 1-phosphatases, inositol monophosphatases (IMPases), 3'-phosphoadenosine 5'-phosphatases (PAPases), and enzymes acting on both inositol 1,4-bisphosphate and PAP (PIPases) (2). They possess a common structural core with the active site lying between $\alpha+\beta$ and α/β domains (3). Li⁺-sensitive phosphatases are putative targets for lithium therapy in the treatment of manic depressive patients (4), whereas FBPases are targets for the development of drugs for the treatment of noninsulin-dependent diabetes (5, 6). In addition, FBPase is required for virulence in *Mycobacterium tuberculosis* and *Leishmania major* and plays an important role in the production of lysine and glutamate by *Corynebacterium glutamicum* (7, 8).

Presently, five different classes of FBPases have been proposed based on their amino acid sequences (FBPases I to V) (9–11). Eukaryotes contain only the FBPase I-type enzyme, but all five types exist in various prokaryotes. Types I, II, and III are primarily in bacteria, type IV in archaea (a bifunctional FBPase/inositol monophosphatase), and type V in thermophilic prokaryotes from both domains (11). Many organisms have more than one FBPase, mostly the combination of types I + II or II + III, but no bacterial genome has a combination of types I and III FBPases (9). The type I FBPase is the most widely distributed among living organisms and is the primary FBPase in *Esche-*

* This work was supported, in whole or in part, by National Institutes of Health Grant GM074942. This work was also supported by Genome Canada (through the Ontario Genomics Institute) and by the United States Department of Energy, Office of Biological and Environmental Research, Contract DE-AC02-06CH11357. The costs of publication of this article were defrayed in part by the payment of page charges. This article must therefore be hereby marked "advertisement" in accordance with 18 U.S.C. Section 1734 solely to indicate this fact.

The atomic coordinates and structure factors (codes 3bih, 3big, 3d1r) have been deposited in the Protein Data Bank, Research Collaboratory for Structural Bioinformatics, Rutgers University, New Brunswick, NJ (<http://www.rcsb.org/>).

[S] The on-line version of this article (available at <http://www.jbc.org>) contains supplemental Fig. 1.

¹ To whom correspondence should be addressed. Tel.: 416-978-4013; Fax: 416-978-8528; E-mail: a.iakounine@utoronto.ca.

² The abbreviations used are: FBPase, fructose-1,6-bisphosphatase; FBP, fructose 1,6-bisphosphate; IMPase, inositol monophosphatase; PAPase, 3'-phosphoadenosine 5'-phosphatase; PIPase, enzyme acting on both inositol-1,4-bisphosphate and 3'-phosphoadenosine 5'-phosphate; CHES, 2-(cyclohexylamino)ethanesulfonic acid; PDB, Protein Data Bank.

richia coli, most bacteria, a few archaea, and all eukaryotes (9, 11–15). The type II FBPases are represented by the *E. coli* GlpX and FBPase F-I from *Synechocystis* PCC6803 (9, 16); type III is represented by the *Bacillus subtilis* FBPase (17); type IV is represented by the dual activity FBPases/inosine monophosphatases FbpA from *Pyrococcus furiosus* (18), MJ0109 from *Methanococcus jannaschii* (19), and AF2372 from *Archaeoglobus fulgidus* (20); and type V is represented by the FBPases TK2164 from *Pyrococcus (Thermococcus) kodakaraensis* and ST0318 from *Sulfolobus tokodai* (10, 21).

Three-dimensional structures of the type I (from pig kidney, spinach chloroplasts, and *E. coli*), type IV (MJ0109 and AF2372), and type V (ST0318) FBPases have been solved (10, 11, 19, 20, 22, 23). FBPases I and IV and inositol monophosphatases share a common sugar phosphatase fold organized in five layered interleaved α -helices and β -sheets (α - β - α - β - α) (2, 19, 24). ST0318 (an FBPase V enzyme) is composed of one domain with a completely different four-layer α - β - β - α fold (10). The FBPases from these three classes (I, IV, and V) require divalent cations for activity (Mg^{2+} , Mn^{2+} , or Zn^{2+}), and their structures have revealed the presence of three or four metal ions in the active site.

E. coli has five Li^+ -sensitive phosphatases as follows: CysQ (a PAPase), SuhB (an IMPase), Fbp (a FBPase I enzyme), GlpX (a FBPase II), and YggF (an uncharacterized protein) (see the Pfam data base). CysQ is a 3'-phosphoadenosine 5'-phosphatase involved in the cysteine biosynthesis pathway (25, 26), whereas SuhB is an inositol monophosphatase (IMPase) that is also known as a suppressor of temperature-sensitive growth phenotypes in *E. coli* (27, 28). Fbp is required for growth on gluconeogenic substrates and probably represents the main gluconeogenic FBPase (12). This enzyme has been characterized both biochemically and structurally and shown to be inhibited by low concentrations of AMP (IC_{50} 15 μM) (11, 29, 30). The *E. coli* GlpX, a class II enzyme FBPase, has been shown to possess a Mn^{2+} -dependent FBPase activity (9). The increased expression of *glpX* from a multicopy plasmid complemented the Fbp⁻ phenotype; however, the *glpX* knock-out strain grew normally on gluconeogenic substrates (succinate or glycerol) (9).

In this study, we present the first structure of a class II FBPase, the *E. coli* GlpX, in a free state and in the complex with FBP + metals or phosphate. We have demonstrated that the fold of GlpX is similar to that of the lithium-sensitive phosphatases. We have identified the GlpX residues important for activity and proposed a catalytic mechanism. We have also showed that YggF is a third FBPase in *E. coli*, which has distinct catalytic properties and is more sensitive than GlpX to the inhibition by lithium or phosphate.

EXPERIMENTAL PROCEDURES

Gene Cloning, Overexpression, and Purification of GlpX and YggF—The GlpX open reading frame was PCR-amplified using chromosomal DNA of the *E. coli* DH5 α strain and the cloning primers containing the restriction sites for BamHI and NdeI and was cloned into the modified pET15b vector (Novagen) in which the tobacco etch virus protease cleavage site replaced the thrombin cleavage site, and a double stop codon was intro-

duced downstream from the BamHI site (31). The overexpression plasmid was transformed into the *E. coli* BL21 (DE3) Gold strain (Stratagene). The YggF overexpressing plasmid was obtained from the Genobase collection (32). GlpX and YggF were overexpressed in *E. coli* and purified using metal-chelate affinity chromatography on nickel affinity resin (Qiagen) with a high yield (>50 mg/liter culture) and homogeneity (>95%) as described previously (31). Purified proteins were concentrated using a centrifugal membrane concentrator (Millipore), frozen as drops in liquid nitrogen and stored at $-80^{\circ}C$.

Gel filtration analysis of the oligomeric state of GlpX and YggF was performed with a Superdex-75 16/60 column (Amersham Biosciences) equilibrated with 10 mM HEPES-K (pH 7.5) and 0.2 M NaCl using AKTA FPLC (Amersham Biosciences). The column was calibrated with ribonuclease A (13.7 kDa), chymotrypsinogen (25 kDa), ovalbumin (43 kDa), albumin (67 kDa), and aldolase (158 kDa).

Enzymatic Assays—Phosphatase activity against fructose 1,6-bisphosphate or other substrates (glucose 1,6-bisphosphate, ribulose 1,5-bisphosphate, and fructose 2,6-bisphosphate, all from Sigma) was measured spectrophotometrically using the Malachite Green reagent (33) essentially as described previously (34). The reaction mixture (0.16 or 0.8 ml) contained 50 mM CHES-K buffer (pH 9.0), 2 mM $MnCl_2$, 0.1 mM fructose 1,6-bisphosphate, and 0.07–0.2 μg of enzyme. After 20 min of incubation at $37^{\circ}C$, the reaction was terminated by the addition of Malachite Green reagent (0.04 or 0.2 ml) (33), and the production of P_i was measured at 630 nm. For determination of the K_m and V_{max} , the assays contained substrates at concentrations of 0.02–0.5 mM. Kinetic parameters were determined by nonlinear curve fitting from the Lineweaver-Burk plot using GraphPad Prism software (version 4.00 for Windows, GraphPad Software, San Diego, CA). The effect of inorganic phosphate on FBPase activity of GlpX and YggF was measured using the continuous assay with phosphoglucosomerase and glucose-6-phosphate dehydrogenase (9).

Site-directed Mutagenesis of GlpX—Site-directed mutagenesis was performed using the QuikChangeTM site-directed mutagenesis kit (Stratagene) according to the manufacturer's protocol. The amino acids selected to be mutated were all changed to alanine. DNA encoding wild-type GlpX cloned into the modified pET15b was used as a template for mutagenesis. The standard PCR mixture contained 50–100 ng of template DNA and 150–250 ng of each mutagenizing primer. The methylated plasmid was digested with DpnI, and 4 μl of each reaction were used to transform competent DH5 α cells. Plasmid was purified from the resulting ampicillin-resistant colonies using the QIAprep Spin mini prep kit (Qiagen), and all mutations were verified by DNA sequencing. Verified plasmids containing the desired mutations were transformed into the *E. coli* BL21 (DE3) strain, and the mutant GlpX proteins were overexpressed and purified in the same manner as the wild-type GlpX.

Protein Crystallization and Data Collection—Crystals of GlpX were grown at $21^{\circ}C$ by the hanging drop vapor diffusion method with 2 μl of protein sample mixed with an equal volume of the reservoir buffer as described previously (35). The crystals of the wild-type GlpX grew after 1–2 weeks in the presence of

Fructose-1,6-bisphosphatases GlpX and YggF

7% polyethylene glycol 8000, 0.2 M $(\text{NH}_4)_2\text{SO}_4$, and 0.1 M sodium acetate (pH 4.4). The crystals of the GlpX D61A complex with fructose 1,6-bisphosphate were obtained by crystallization in the presence of 28% polyethylene glycol 400, 0.2 M CaCl_2 , 0.1 M HEPES-Na (pH 7.5), and 10 mM fructose 1,6-bisphosphate, whereas the complex of the GlpX D61A with phosphate was crystallized in 30% polyethylene glycol 4000, 0.2 M NH_4 acetate, and 0.1 M sodium citrate (pH 5.6). For diffraction studies, the crystals were stabilized with the crystallization buffer supplemented with 20% ethylene glycol as a cryoprotectant and flash-frozen in liquid nitrogen.

Structure Determination—The first apo-structure of GlpX (PDB code 1ni9) was solved using multiwavelength anomalous dispersion. Diffraction data were collected at 100 K on a single crystal on the 19-ID beamline of the Structural Biology Center at the Advanced Photon Source (36) at the peak and inflection wavelength of the selenium K absorption edge as well as a remote wavelength. Data were integrated using d*TREK and scaled with HKL2000 (37). The selenium sites were found with SOLVE (38), followed by phase improvement by density modification and automated building to generate an initial model using RESOLVE (39, 40). Diffraction data for native crystals of apo-GlpX in space group P422 (PDB code 3bih), GlpX D61A plus phosphate (PDB code 3big), and GlpX D61A plus FBP (PDB code 3d1r) were collected at 100 K on a Rigaku Micromax-007 rotating anode generator equipped with Osmic confocal “blue” optics, and diffraction intensities were recorded on a Rigaku R-AXIS IV++ image plate system (Table 2). The resulting diffraction data were integrated and scaled using HKL2000 (37), and the structures were solved using molecular replacement using the protein atoms from the first GlpX structure (PDB code 1ni9). Molecular replacement was performed using MOLREP (41) for the apo-GlpX and phosphate-bound complex and PHASER (42) for the FBP-bound structure. Initial protein models were then improved with several rounds of manual building using COOT (43) and restrained refinement against a maximum likelihood target using REFMAC (44) within the CCP4 program suite (45), with 5% of the reflections randomly excluded as an R_{free} test set.

Protein Data Bank Accession Codes—Coordinates and structure factors have been deposited with accession codes 1ni9 and 3bih (wild-type GlpX, apo-structure), 3d1r (GlpX D61A + FBP complex), and 3big (GlpX D61A + phosphate complex).

RESULTS AND DISCUSSION

***E. coli* Has Two Genes Encoding the Type II (GlpX-like) FBPases**—In the *E. coli* genome, the *glpX* gene forms an operon (*glpFKX*) with *glpF* (a glycerol transport facilitator) and *glpK* (a glycerol kinase). This operon is one of five operons of the *glp* regulon involved in the growth of *E. coli* on glycerol (9). A BLAST analysis of the *E. coli* genome using the GlpX sequence (336 amino acids) as a query identified the uncharacterized protein YggF (321 amino acids), which shares 58% sequence identity with GlpX. The *yggF* gene is part of a large operon (*cmtBA* and *yggPFDC*), which encodes a mannitol phosphoenolpyruvate-dependent transferase (CmtB and CmtA), a predicted dehydrogenase (YggP), a predicted transcriptional regulator (YggD),

and a putative kinase (YggC). The role of YggF in *E. coli* is unknown, although GlpX is likely to be involved in gluconeogenesis during growth on glycerol (9). A BLAST search of the sequenced genomes with the *E. coli* GlpX as a query revealed that the type II FBPases are quite conserved enzymes with over 100 sequences showing 50% or higher sequence identity. Besides *E. coli*, two genes encoding a type II FBPase were found in many strains of *Shigella* and *Bacillus*.

Sequence alignment of GlpX and YggF with the experimentally verified type II FBPases from *M. tuberculosis* (46), *C. glutamicum* (47), and *Synechocystis* PCC 6803 (16) (42–44% sequence identity) identified over 50 conserved residues (Fig. 1). These sequences show the presence of four blocks of conserved residues (⁵⁴VIGE⁵⁹, ⁶³APML⁶⁶, ⁸³AVDP⁸⁶, and ¹⁸⁶DGDV¹⁸⁹). The block-3 is a part of the Li^+ -sensitive phosphatase motif DP(I/L)D(G/S)(T/S) (Fig. 1) that has been shown by crystallographic and mutational studies to bind metals and participate in catalysis (2, 48). Previously, it has been mentioned that the presence of this sequence motif in proteins is not sufficient to identify family members *per se* (2). However, the FBPase II sequences revealed no presence of the extended Li^+ -sensitive phosphatase motif with the conserved combinations of EE, WD, or GG (2) suggesting that the class II FBPases are evolutionarily distant from the main group of Li^+ -sensitive phosphatases.

Biochemical Characterization of GlpX and YggF—Purified GlpX and YggF exhibited a high fructose-1,6-bisphosphatase activity, a low activity toward glucose 1,6-bisphosphate (0.11–0.39 $\mu\text{mol}/\text{min mg}$ protein), and no activity against ribulose 1,5-bisphosphate, fructose 2,6-bisphosphate, or fructose 1-phosphate. With fructose 1,6-bisphosphate as substrate, both proteins had maximal activity at pH 7.5–8.0 (data not shown) and required a divalent metal cation for activity. When tested with a range of divalent cations (Mg^{2+} , Mn^{2+} , Co^{2+} , Ni^{2+} , Ca^{2+} , Cu^{2+} , and Zn^{2+} ; 1 mM final concentration), only Mn^{2+} supported activity of both proteins. This is in contrast to FBPases from other classes, which can be activated by Mg^{2+} , Mn^{2+} , or Zn^{2+} (21, 49). GlpX had a slightly higher affinity to Mn^{2+} (K_D 0.6 mM) than YggF (K_D 1.0 mM) (Table 1). Moreover, GlpX showed higher activity and affinity to fructose 1,6-bisphosphate resulting in three times higher catalytic efficiency (Table 1). With this substrate, both proteins showed saturation kinetics with sigmoidal saturation curve with a Hill coefficient n_H 2.0–2.1 indicating positive cooperativity in substrate binding. When compared with other *E. coli* FBP phosphatases, both GlpX and YggF showed lower substrate affinity and catalytic efficiency than those of Fbp, but they were more efficient in FBP hydrolysis than YaeD and YbhA, which belong to the haloacid dehalogenase-like phosphohydrolase superfamily (Table 1).

The activity of YggF was slightly increased (40–50%) by the addition of 1 mM dithiothreitol, whereas 1 mM ATP reduced activity by 40% (data not shown). All other tested effectors (AMP, ADP, PEP, and glycerol 3-phosphate; 1 mM each) produced no significant effect on the activity of both YggF and GlpX (even in the incubation assays described in Ref. 50). These results are similar to that obtained for the class II-like FBPase from *M. tuberculosis* (46). KCl (50 mM) slightly stimulated

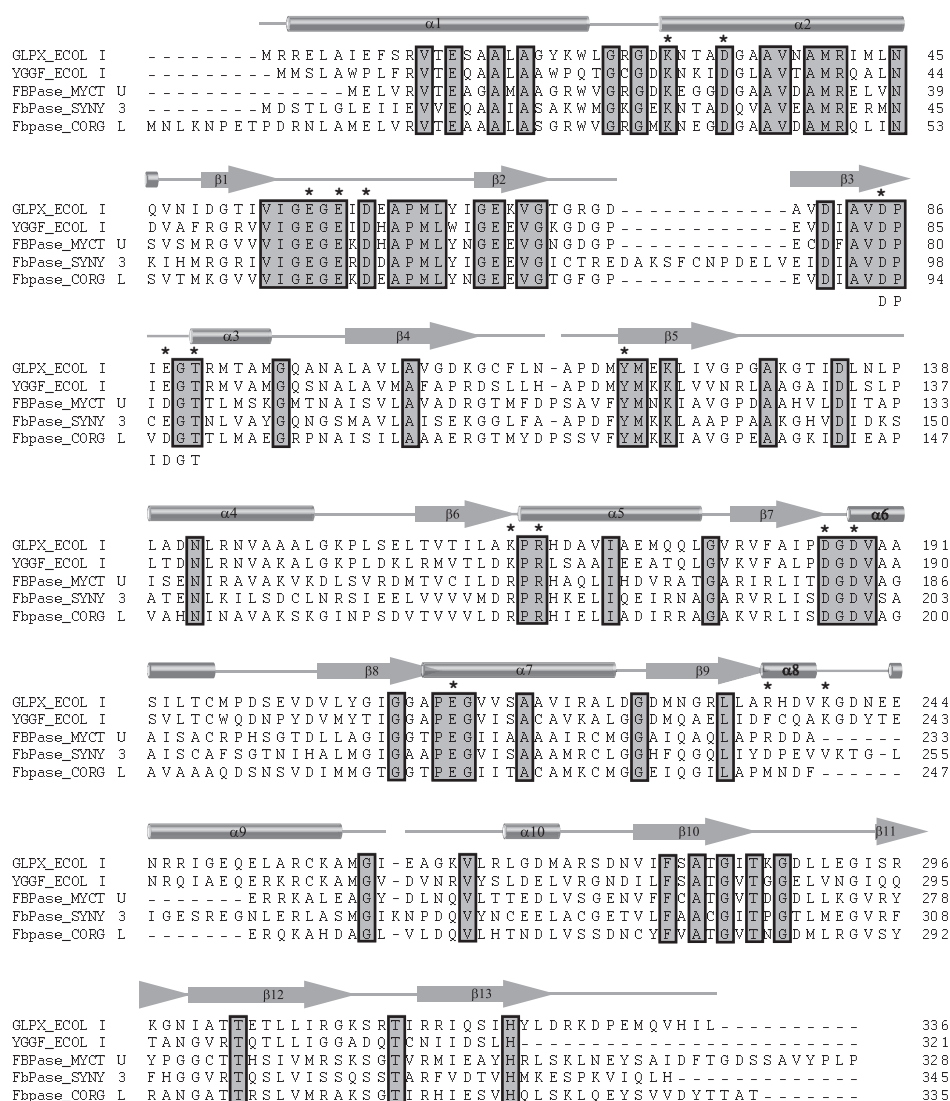


FIGURE 1. Structure-based sequence alignment of the *E. coli* GlpX and other experimentally verified class II FBPs. The secondary structure elements of GlpX are shown above the alignment. Residues conserved in all aligned class II FBPs are boxed and highlighted in gray. The GlpX residues mutated to Ala in this work are marked with an asterisk above the alignment. The lithium-sensitive phosphatase motif (DPIIDGT) is shown below the alignment. The compared proteins are *E. coli* GlpX (P0A9C9), *E. coli* YggF (P21437), *M. tuberculosis* FBPase Rv1099c (O53447), *Synechocystis* PCC6803 FBPase F-1 (P73922), and *C. glutamicum* FBPase (A4QCY3).

TABLE 1

Kinetic parameters of the *E. coli* FBPs, GlpX, YggF, Fbp, YaeD, and YbhA

Protein	Variable substrate	K_m	V_{max}^a	k_{cat}	k_{cat}/K_m
		mM	units/mg	s^{-1}	$M^{-1}s^{-1}$
GlpX (wild type)	FBP	0.07 ± 0.002	8.8 ± 0.1	5.7 ± 0.1	0.9×10^5
GlpX (K29A)	FBP	0.06 ± 0.008	21.6 ± 2.2	14.0 ± 1.0	2.6×10^5
GlpX (E59A)	FBP	0.1 ± 0.003	1.6 ± 0.1	1.1 ± 0.06	1.06×10^3
GlpX (D186A)	FBP	0.2 ± 0.02	1.8 ± 0.1	1.2 ± 0.06	6.0×10^3
GlpX (R235A)	FBP	0.2 ± 0.03	8.4 ± 0.9	5.4 ± 0.6	2.7×10^4
GlpX (K239A)	FBP	0.1 ± 0.03	11.7 ± 1.4	7.5 ± 0.9	0.6×10^5
YggF (wild type)	FBP	0.1 ± 0.01	4.0 ± 0.3	2.5 ± 0.2	2.4×10^4
GlpX (wild type)	Mn ²⁺	0.6 ± 0.04	4.5 ± 0.2	2.9 ± 0.11	0.5×10^4
YggF (wild type)	Mn ²⁺	1.0 ± 0.02	4.5 ± 0.1	2.9 ± 0.05	0.3×10^4
Fbp ^a	FBP	0.02 ± 0.002	24.2	14.6 ± 0.8	9.7×10^5
YaeD ^b	FBP	0.4 ± 0.06	0.5 ± 0.02	0.2 ± 0.01	0.5×10^3
YbhA ^b	FBP	2.4 ± 0.2	9.7 ± 0.2	5.3 ± 0.1	2.2×10^3

^a Data are from Kelley-Loughnane *et al.* (30).

^b Data are from data from Kuznetsova *et al.* (61).

activity of GlpX (20%), but produced a strong inhibiting effect on YggF (20% residual activity). Most of the Li⁺-sensitive phosphatases are strongly inhibited by submillimolar concentrations of Li⁺ (IC₅₀ 0.07–0.3 mM) (2, 3, 47, 51–53). We found that both GlpX and YggF were sensitive to Li⁺ with an IC₅₀ of 70 mM for GlpX and 15.8 mM for YggF (supplemental Fig. 1). Therefore, like the dual specificity IMPase/FBPase enzymes AF2372 and MJ0109 (20, 54), the *E. coli* class II FBPs belong to the group of more resistant Li⁺-sensitive phosphatases. In addition, FBPase activity of both GlpX and YggF was inhibited by low concentrations of inorganic phosphate (IC₅₀ 3.0 and 1.2 mM, respectively) (supplemental Fig. 1). Thus, in *E. coli* both type II FBPs are distinct from FBPase I, which is highly sensitive to inhibition by AMP and requires Mg²⁺ for activity (29).

Crystal Structure of the Ligand-free GlpX—The crystal structure of *E. coli* GlpX was solved to 2.0 Å resolution in space group P4₁2₁2 (PDB code 1ni9) using multiwavelength anomalous dispersion on a crystal containing selenomethionine-substituted protein. However, the first structure was not optimal as several regions predicted to contain strands and helices were disordered. Therefore, the structure of apo-GlpX was solved in another space group (P4₂2, PDB code 3bih), and this structure contained many more ordered regions even though it was

solved at a similar resolution (2.1 Å) (Table 2). The structure demonstrated that two subunits of GlpX create an elongated dimer (Fig. 2). The elongated shape of the GlpX dimer is a likely reason for the anomalously high native molecular mass of GlpX obtained in gel filtration experiments, 118 kDa (predicted monomer mass of 36 kDa). Gel filtration analysis of the oligomeric state of YggF revealed that it is likely to exist as a dimer in solution, 76 kDa (predicted monomer mass of 34.3 kDa). Two GlpX subunits are connected by β -sheet interactions between the last β -strands (β 15) creating a joint six-stranded anti-parallel β -sheet (Fig. 2). The dimerization interface is stabilized mainly by these β -sheet interactions and by a salt bridge between Arg³ and Glu⁸ from the first helix of two monomers.

The GlpX monomer has a compact, globular shape with two α/β -type domains arranged as a multilayered sandwich (α/β

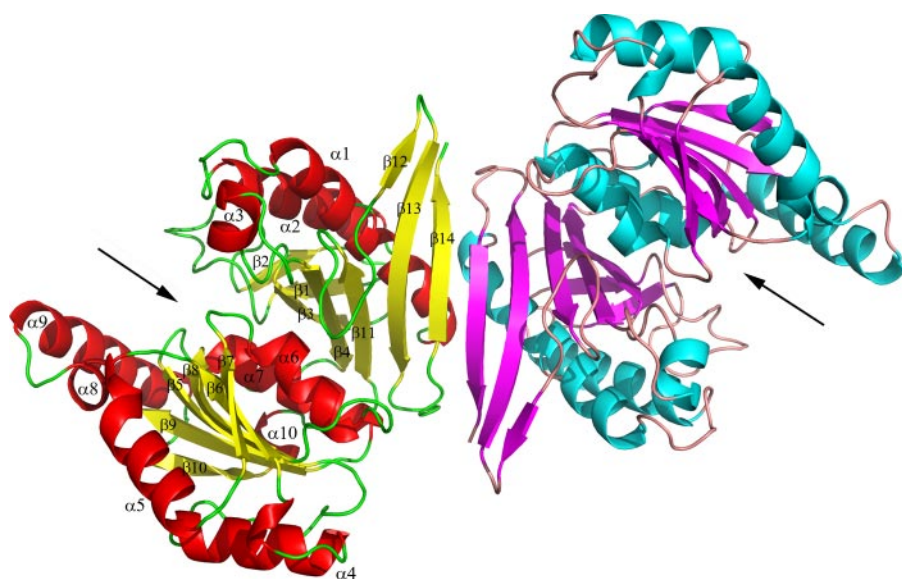


FIGURE 2. **Crystal structure of GlpX, overall structure of the GlpX dimer.** Protein monomers are shown in different colors. In each monomer, the potential active site is located between two protein domains and is indicated by the *black arrow*. In both monomers, the α/β layers are shown in different colors, and in one monomer the secondary structure elements are labeled.

$\alpha/\beta/\alpha$) (Fig. 3A). The two-layer domain A (the left domain on Fig. 3A) includes the sequences from the N-terminal (Arg²–Asp¹⁰⁸) and C-terminal parts (Val²⁷⁸–Tyr³²³) of GlpX and is formed by the antiparallel β -sheet with eight β -strands, which is partially wrapped around two long α -helices (a hot dog-like configuration). The domain B (the right domain on Fig. 3A) includes the sequences from the central part of GlpX (Lys¹⁰⁹–Asn²⁷⁷) and adopts a three-layered $\alpha/\beta/\alpha$ -sandwich configuration with the β -strands forming a central, mostly parallel β -sheet (five β -strands). Domains A and B are joined by two closely located connecting loops (β 4– β 5 and α 10– β 11, 10 and 5 residues long). A well defined cleft is present

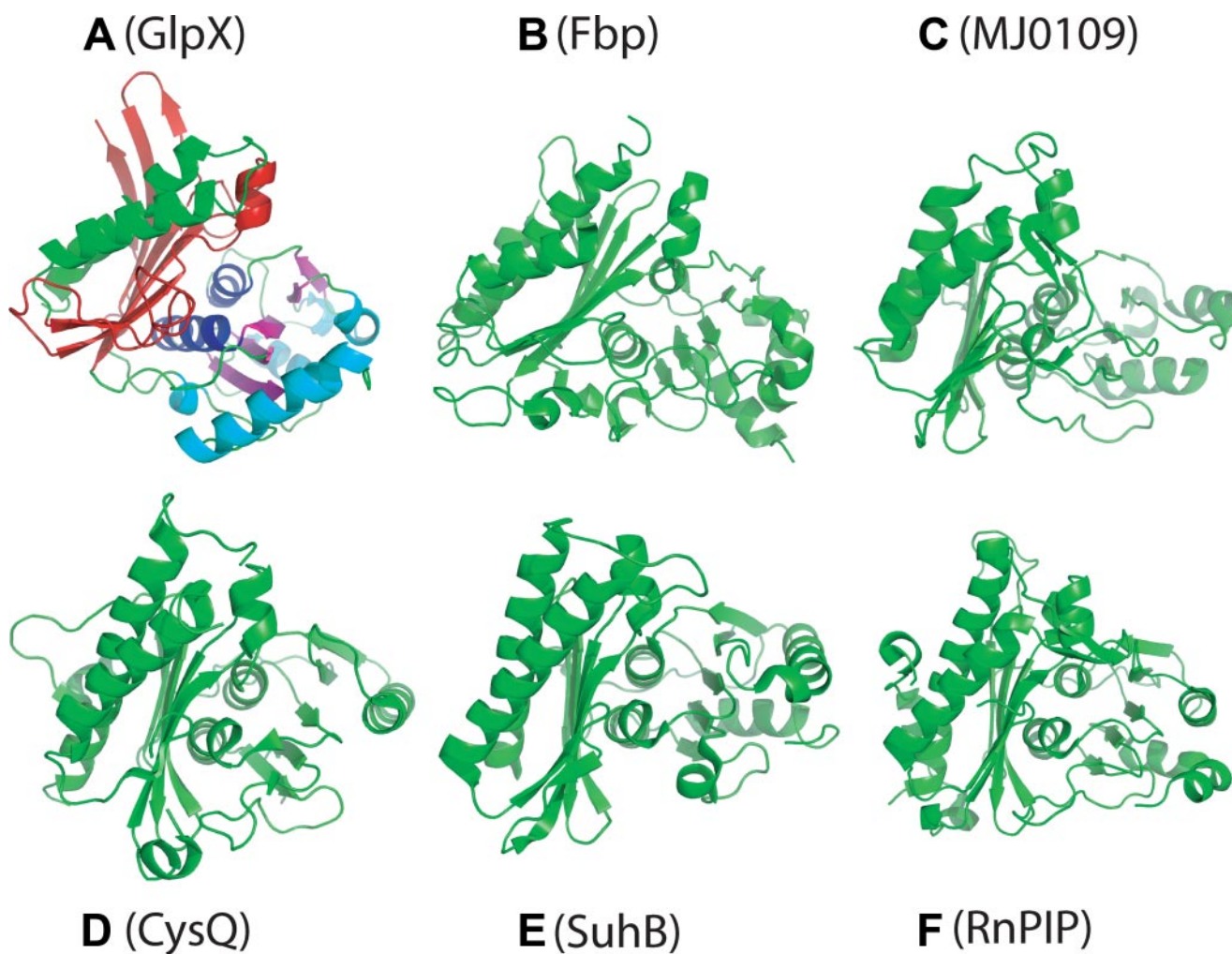


FIGURE 3. **Monomer structures of GlpX and other FBPases and Li⁺-sensitive phosphatases.** A, *E. coli* GlpX (FBPase II; PDB code 3bih); B, *E. coli* Fbp (FBPase I; PDB code 2q8m); C, MJ0109 (FBPase IV; PDB code 1dk4); D, *E. coli* SuhB (IMPase; PDB code 2qfl); E, CysQ from *B. thetaiotaomicron* (PAPase; PDB code 3b8b); and F, RnPIP (PIPase; PDB code 1jp4). All of the polypeptides are shown in equivalent orientations revealing the presence of a five-layered $\alpha\text{-}\beta\text{-}\alpha\text{-}\beta\text{-}\alpha$ structure. The α/β layers of GlpX are shown in different colors: α 1, green; β 1, red; α 2, blue; β 2, magenta; α 3, cyan.

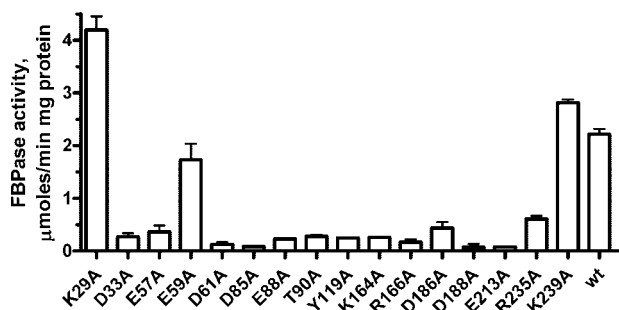


FIGURE 4. Alanine replacement mutagenesis of GlpX, FBPAse activity of purified mutant proteins. The reaction mixtures contained 0.1 mM FBP and 0.1–0.5 μg of GlpX; the assays were performed as described under “Experimental Procedures.”

between the domains, which accommodates many conserved residues and represents a putative active site of GlpX (Fig. 2 and Fig. 3A).

A Dali search identified the rat inositol-polyphosphate 1-phosphatase (RnPIP) as the best hit (PDB 1jp4, Z-score 11.2, root mean square deviation 3.2 Å). Previous work has found that the mammalian fructose-1,6-bisphosphatase and inositol monophosphatase (IMPase) share a similar secondary structure topology even though their sequences show low similarity (55). Both enzymes have a layered $\alpha\beta\alpha\beta\alpha$ -type structure and almost identical five metal-binding carboxylate residues. Analysis of the presently available structures of inositol monophosphatases (RnPIP, *E. coli* SuhB, and CysQ from *Bacteroides thetaiotaomicron*) and three classes of FBPAses (I, *E. coli* Fbp; II, *E. coli* GlpX; and IV, MJ0109) shows that they share the same secondary structure topology ($\alpha\beta\alpha\beta\alpha$) (Fig. 3). In these structures, the first layer has two (GlpX, MJ0109, and RnPIP) or three (Fbp) nearly parallel α -helices, whereas the second layer consists of mostly anti-parallel β -sheets of six or eight strands. The two next middle layers (two parallel α -helices and four or five stranded β -sheet) are almost perpendicular to the second layer β -sheet, whereas the three to five α -helices of the fifth layer have different orientations (Fig. 3). The unique feature of the GlpX fifth layer is the presence of an additional long α -helix (α_{10}), which is parallel to the long α_2 helix of the first layer. Thus, although IMPases and FBPAse classes I, II, and IV have a very low overall sequence similarity, their structural similarity suggests that they have a common evolutionary origin and catalytic mechanism.

Mutational Studies of GlpX—In the GlpX structure, many conserved residues are located within or close to the large cavity located between two protein domains, which contains a putative active site (Fig. 2). To identify the active site residues involved in FBP hydrolysis, we have mutated 12 conserved and 4 semi-conserved residues of GlpX to Ala. 12 purified mutant proteins showed a greatly reduced FBPAse activity suggesting that they are involved in substrate binding (FBP and metals) or catalysis (Fig. 4). The E59A mutant exhibited both reduced activity and reduced substrate affinity (Table 1). The GlpX structure shows that the side chain of Glu⁵⁹ is potentially involved in the inter-domain interaction through hydrogen bonding with the conserved Arg²⁵⁵ (4.3 Å). The side chain of the conserved Asp⁶¹ might also be involved in the inter-domain

interaction (with Arg²⁵⁵), and D61A mutant protein showed very low FBPAse activity (Fig. 4). K29A retained the wild-type level of substrate affinity, whereas its activity increased to three times the level of the wild-type protein (Fig. 4 and Table 1). The GlpX structure shows that Lys²⁹ is located on the edge of the putative active site and its side chain might interfere with substrate binding and product release. Therefore, the removal of the Lys²⁹ side chain would open the catalytic cleft of GlpX, thereby increasing the rate of substrate binding/product release and consequently the overall reaction rate. Both the D186A and R235A mutant proteins had reduced affinity to FBP (Table 1) suggesting that they are involved in substrate binding. The side chain of Lys²³⁹ is positioned close to that of Arg²³⁵, but perhaps is not involved in substrate coordination because the K239A protein demonstrated the wild-type activity and substrate affinity (Table 1).

Crystal Structure of the GlpX Complexes with FBP or Phosphate—The GlpX D61A mutant protein was crystallized in the presence of FBP, Ca²⁺, and Mg²⁺, and its structure revealed the presence of three metal atoms and FBP in the predicted active site (Fig. 5A and Table 2). In general, the active site of GlpX is less open than that of the dual activity inositol monophosphatases/FBPAses (e.g. AF2372), consistent with the narrow substrate specificity of GlpX. The FBP molecule is bound in a closed ring form and coordinated by the interactions with side chains and main chain amide groups of several conserved residues (Fig. 5A). The 6-phosphate group of FBP interacts with the side chains of Tyr¹¹⁹ (2.7 Å), Lys¹⁶⁴ (2.8 Å), and Arg¹⁶⁶ (2.6 Å). Similar combinations of the Arg, Lys, and Tyr residues are present in the structures of other FBPAses (e.g. Lys¹⁶⁷, Arg¹⁶⁸, and Arg¹⁷⁰ in MJ0109) but are absent in inositol monophosphatases, suggesting that these residues determine the substrate specificity of FBPAses to FBP. The FBP 4-OH group is recognized by the side chain of Asp¹⁸⁸ (2.6 Å) and the main chain amide of Gly²¹⁰ (2.9 Å), the 3-OH group by the Glu⁸⁸ side chain (2.6 Å) and the main chain amide of Asp¹⁸⁸ (2.7 Å), and the 2-OH group by the side chain of Asp¹⁸⁶ (2.6 Å) and the main chain amide of Gly¹⁸⁷ (3.1 Å) (Fig. 5A). The oxygen atoms of the 1-phosphoryl group of FBP (a removable group) are liganded to the main chain amide of Gly⁸⁹ (2.8 Å) and the side chains of Asp¹⁸⁶ (3.4 Å) and Thr⁹⁰ (3.3 Å).

The crystal structure of the GlpX-FBP complex revealed the presence of three metal cations in the active site, which were identified as Ca²⁺ or Mg²⁺, because both were present in the crystallization solution (metal ions with smaller radii were identified as Mg²⁺) (Fig. 5A). The metal-1 (Mg²⁺) is coordinated by the FBP phosphoryl 6 oxygen (2.2 Å) and is located 4.3 Å from the P1 oxygens (Fig. 5A). The other two metals (Ca1 and Ca2) are located close to each other (5.6 Å) and to the phosphoryl 1 oxygens of the substrate (4.7 Å for Ca1 and 6.6 Å for Ca2) (Fig. 5A). Ca1 is bound to the side chains of Glu⁸⁸ (2.4 Å), Glu²¹³ (2.4 Å), and Asp⁸⁵ (2.4 Å and 2.5 Å), whereas Ca2 is liganded to the side chains of Glu⁵⁷ (2.6 Å) and Asp³³ (2.2 Å). Thus, the metal-coordinating residues of GlpX are similar to that of RnPIP (56) and Hal2p (3) suggesting that GlpX might have a similar catalytic mechanism.

Fructose-1,6-bisphosphatases GlpX and YggF

Previous work on the *E. coli* GlpX demonstrated that inorganic phosphate competitively inhibits FBPase activity with a K_i of 0.35 mM (9). The structure of the GlpX-phosphate complex

revealed the presence of phosphate bound to the enzyme active site (Fig. 5B). The phosphate molecule occupies the position of the phosphate 6 of fructose-1,6-bisphosphatase and is coordinated

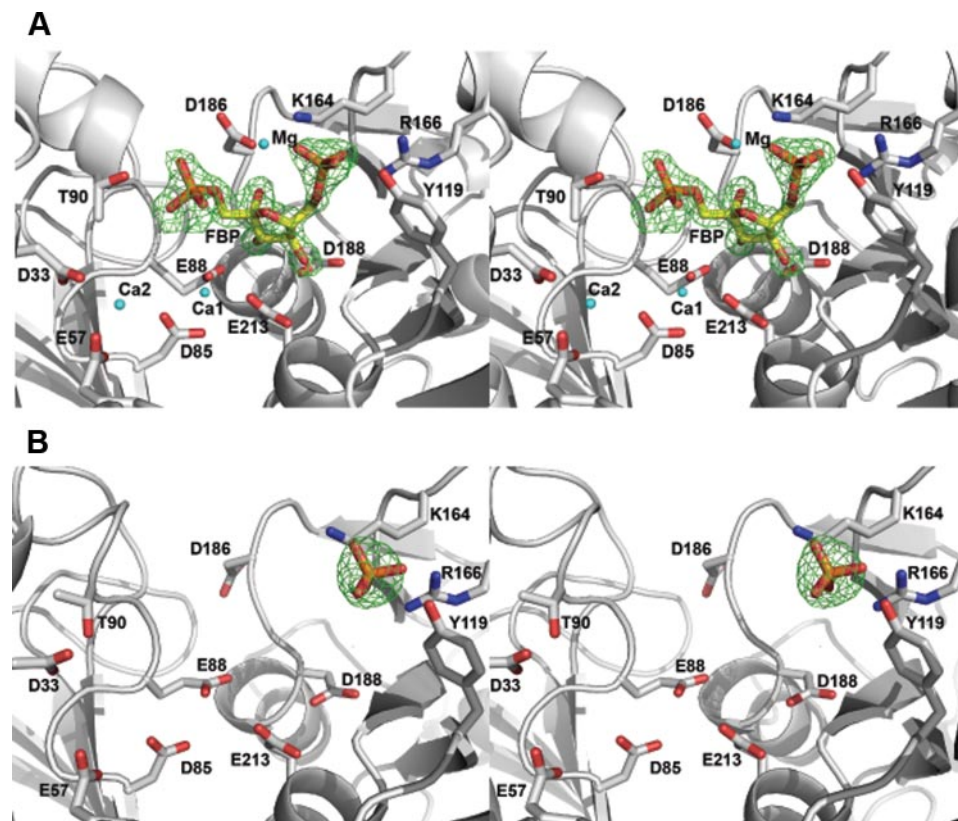


FIGURE 5. **Wide-eye stereo view of the GlpX active site.** A, FBP bound in the GlpX-FBP complex (PDB code 3d1r); B, phosphate bound in the GlpX-phosphate complex (PDB code 3big). The ligand, metal ions (Mg, Ca1, and Ca2) and selected residues of GlpX (D61A) in contact with the ligand and metal ions (cyan spheres) are shown as a stick diagram along with a GlpX ribbon (gray). Difference electron density was calculated by removing the fructose 1,6-bisphosphate from the final model, followed by several rounds of maximum likelihood refinement using Refmac5. The resulting $F_o - F_c$ map was contoured at 4.2σ .

TABLE 2

Crystallographic data collection and model refinement statistics

Values in parentheses are for the highest resolution shell.

	GlpX wild type (apo) (PDB 3bih)	GlpX D61A + FBP (PDB 3d1r)	GlpX D61A + phosphate (3big)
Data collection			
Space group	P422	P422	P422
Cell dimensions <i>a</i> , <i>c</i> (Å)	<i>a</i> = 91.4, <i>c</i> = 86.5	<i>a</i> = 91.3, <i>c</i> = 84.9	<i>a</i> = 91.3, <i>c</i> = 86.4
Wavelength	1.54178	1.54178	1.54178
Resolution	50-2.1 Å (2.18-2.1 Å)	50-1.85 Å (1.90-1.85 Å)	50-1.81 Å (1.87-1.81 Å)
R_{merge}	0.073 (0.525)	0.060 (0.464)	0.056 (0.55)
$I/\sigma I$	30.4 (3.1)	40.1 (7.2)	44.5 (2.6)
Completeness (%)	99.8 (98.1)	100.0 (100.0)	99.3 (92.3)
Redundancy	9.2 (8.0)	13.5 (13.1)	12.0 (4.7)
Refinement			
Resolution	39.0 to 2.1 Å	28.65 to 1.85 Å	40.9 to 1.85 Å
No. of reflections	34,514	29,726	30,207
$R_{\text{work}}/R_{\text{free}}$	0.188/0.250	0.173/0.212	0.189/0.239
No. of atoms			
Protein	2403	2403	2423
Major ligand		20	
Other ligands/ion		9	5
Solvent	159	322	248
Root mean square deviations			
Bond lengths (Å)	0.018	0.017	0.018
Bond angles (°)	1.43	1.55	1.50
Ramachandran plot			
Most favored (%)	90.8	92.9	92.2
Additionally allowed (%)	8.1	7.1	7.8
Disallowed (%)	0.6	0	0

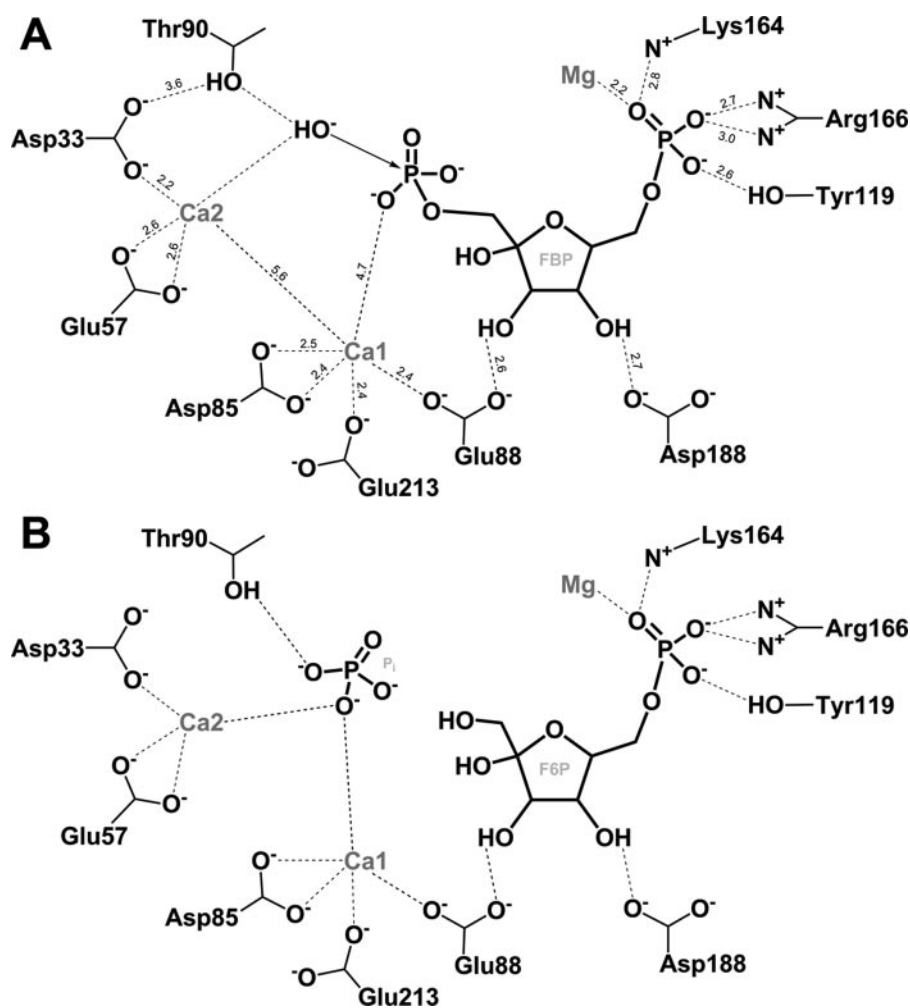


FIGURE 6. A diagram showing the coordination of FBP in the active site of GlpX and the proposed reaction mechanism of FBP hydrolysis by GlpX. A, activation of the catalytic water molecule and nucleophilic attack. The Ca^{2+} -1 ion (Ca1) is assumed to be responsible for the phosphate coordination and charge stabilization during the transition state. The Ca^{2+} -2 ion (Ca2) together with the network of the conserved Thr⁹⁰ and Asp³³ are proposed to be responsible for the activation of the nucleophilic water molecule. The numbers represent interatomic distances in Å. B, products formation and release (P_i , inorganic phosphate; F6P, fructose 6-phosphate). The leaving phosphate group is coordinated by the interactions with two metal ions (Ca1 and Ca2) and the Thr⁹⁰ hydroxyl.

stabilizing the negative charge on the leaving group, whereas the second metal ion coordinates the nucleophilic water (3, 59, 60). The hydrogen bonding with the nearby Thr (or Ser) and carboxylate (Glu or Asp) residues would activate this water molecule. More recently, the second model with three metals was proposed for the catalytic mechanism of Li^+ -sensitive phosphatases (20, 54, 56). In this model, metal ions 1 and 2 are postulated to be involved in substrate binding and stabilization of the intermediate, whereas metal ions 2 and 3 are postulated to be responsible for the coordination of the water nucleophile. In the GlpX-FBP structure, there are three metals bound in the active site, but the metal-1 (Mg^{2+} , liganded to phosphate 6) seems not to be involved in catalysis (Fig. 5A). This suggests that GlpX and other class II FBPases are likely to use a two-metal ion-assisted mechanism for the hydrolysis of FBP similar to that described for the yeast Hal2p PAPase (3).

In the proposed GlpX mechanism, the Ca1 ion is assumed to assist in the FBP binding, as well as in phosphate coordination

and charge stabilization during the transition state. The nucleophilic water molecule would be coordinated by the Ca2 and by the side chain of the conserved Thr⁹⁰ (Thr¹⁴⁷ in Hal2p), which is itself activated by a hydrogen bond with the conserved Asp³³ (Asp⁴⁹ in Hal2p) (Fig. 6). There are two water molecules in the vicinity of the phosphorus 1 atom (W3544 and W3774), which are positioned 2.2–4.7 Å to the Ca2 and Thr⁹⁰ and might function as a nucleophilic water in the hydrolysis of the phosphoester bond. The interaction of the side chains of the conserved Thr and Asp (Thr⁹⁰ and Asp³³ in GlpX) seems to be characteristic for the reaction mechanism of Li^+ -sensitive phosphatases (3). This interaction increases the nucleophilicity of the Thr hydroxyl oxygen and results in the formation of the hydroxyl nucleophile (Fig. 6). The direct involvement of Thr⁹⁰ in the GlpX catalysis is supported by the results of our mutagenic studies (Fig. 4). The emerging hydroxyl ion would subsequently attack the phosphate 1 phosphorus atom of FBP generating a transition intermediate stabilized by the interaction with the Ca1 ion. Thus, the crystal structure of GlpX has demonstrated that its core fold is equivalent to that of Li^+ -sensitive phosphatases and defined important structural determinants for the substrate recognition and catalytic

mechanism of class II FBPases.

Acknowledgments—We thank all members of the Ontario Center for Structural Proteomics (Structural Proteomics in Toronto, SPiT) for their help in conducting these experiments.

REFERENCES

- Horecker, B. L., Melloni, E., and Pontremoli, S. (1975) *Adv. Enzymol. Relat. Areas Mol. Biol.* **42**, 193–226
- York, J. D., Ponder, J. W., and Majerus, P. W. (1995) *Proc. Natl. Acad. Sci. U. S. A.* **92**, 5149–5153
- Patel, S., Martinez-Ripoll, M., Blundell, T. L., and Albert, A. (2002) *J. Mol. Biol.* **320**, 1087–1094
- Nahorski, S. R., Ragan, C. I., and Challiss, R. A. (1991) *Trends Pharmacol. Sci.* **12**, 297–303
- Wright, S. W., Carlo, A. A., Carty, M. D., Danley, D. E., Hageman, D. L., Karam, G. A., Levy, C. B., Mansour, M. N., Mathiowetz, A. M., McClure, L. D., Nestor, N. B., McPherson, R. K., Pandit, J., Pustilnik, L. R., Schulte, G. K., Soeller, W. C., Treadway, J. L., Wang, I. K., and Bauer, P. H. (2002) *J. Med. Chem.* **45**, 3865–3877

Fructose-1,6-bisphosphatases GlpX and YggF

6. Sassetti, C. M., and Rubin, E. J. (2003) *Proc. Natl. Acad. Sci. U. S. A.* **100**, 12989–12994
7. Naderer, T., Ellis, M. A., Sernee, M. F., De Souza, D. P., Curtis, J., Handman, E., and McConville, M. J. (2006) *Proc. Natl. Acad. Sci. U. S. A.* **103**, 5502–5507
8. Becker, J., Klopprogge, C., Zelder, O., Heinzle, E., and Wittmann, C. (2005) *Appl. Environ. Microbiol.* **71**, 8587–8596
9. Donahue, J. L., Bownas, J. L., Niehaus, W. G., and Larson, T. J. (2000) *J. Bacteriol.* **182**, 5624–5627
10. Nishimasu, H., Fushinobu, S., Shoun, H., and Wakagi, T. (2004) *Structure (Lond.)* **12**, 949–959
11. Hines, J. K., Fromm, H. J., and Honzatko, R. B. (2006) *J. Biol. Chem.* **281**, 18386–18393
12. Fraenkel, D. G., and Horecker, B. L. (1965) *J. Bacteriol.* **90**, 837–842
13. Fraenkel, D. G., Pontremoli, S., and Horecker, B. L. (1966) *Arch. Biochem. Biophys.* **114**, 4–12
14. Sedivy, J. M., Daldal, F., and Fraenkel, D. G. (1984) *J. Bacteriol.* **158**, 1048–1053
15. Sato, T., Imanaka, H., Rashid, N., Fukui, T., Atomi, H., and Imanaka, T. (2004) *J. Bacteriol.* **186**, 5799–5807
16. Tamoi, M., Murakami, A., Takeda, T., and Shigeoka, S. (1998) *Biochim. Biophys. Acta* **1383**, 232–244
17. Fujita, Y., Yoshida, K., Miwa, Y., Yanai, N., Nagakawa, E., and Kasahara, Y. (1998) *J. Bacteriol.* **180**, 4309–4313
18. Verhees, C. H., Akerboom, J., Schiltz, E., de Vos, W. M., and van der Oost, J. (2002) *J. Bacteriol.* **184**, 3401–3405
19. Stec, B., Yang, H., Johnson, K. A., Chen, L., and Roberts, M. F. (2000) *Nat. Struct. Biol.* **7**, 1046–1050
20. Stieglitz, K. A., Johnson, K. A., Yang, H., Roberts, M. F., Seaton, B. A., Head, J. F., and Stec, B. (2002) *J. Biol. Chem.* **277**, 22863–22874
21. Rashid, N., Imanaka, H., Kanai, T., Fukui, T., Atomi, H., and Imanaka, T. (2002) *J. Biol. Chem.* **277**, 30649–30655
22. Xue, Y., Huang, S., Liang, J. Y., Zhang, Y., and Lipscomb, W. N. (1994) *Proc. Natl. Acad. Sci. U. S. A.* **91**, 12482–12486
23. Villeret, V., Huang, S., Zhang, Y., Xue, Y., and Lipscomb, W. N. (1995) *Biochemistry* **34**, 4299–4306
24. Choe, J. Y., Fromm, H. J., and Honzatko, R. B. (2000) *Biochemistry* **39**, 8565–8574
25. Neuwald, A. F., Krishnan, B. R., Brikun, I., Kulakauskas, S., Suziedelis, K., Tomcsanyi, T., Leyh, T. S., and Berg, D. E. (1992) *J. Bacteriol.* **174**, 415–425
26. Fukuda, C., Kawai, S., and Murata, K. (2007) *Appl. Environ. Microbiol.* **73**, 5447–5452
27. Matsuhisa, A., Suzuki, N., Noda, T., and Shiba, K. (1995) *J. Bacteriol.* **177**, 200–205
28. Wang, Y., Stieglitz, K. A., Bubunenko, M., Court, D. L., Stec, B., and Roberts, M. F. (2007) *J. Biol. Chem.* **282**, 26989–26996
29. Babul, J., and Guixé, V. (1983) *Arch. Biochem. Biophys.* **225**, 944–949
30. Kelley-Loughnane, N., Biolsi, S. A., Gibson, K. M., Lu, G., Hehir, M. J., Phelan, P., and Kantrowitz, E. R. (2002) *Biochim. Biophys. Acta* **1594**, 6–16
31. Zhang, R. G., Skarina, T., Katz, J. E., Beasley, S., Khachatryan, A., Vyas, S., Arrowsmith, C. H., Clarke, S., Edwards, A., Joachimiak, A., and Savchenko, A. (2001) *Structure (Lond.)* **9**, 1095–1106
32. Kitagawa, M., Ara, T., Arifuzzaman, M., Ioka-Nakamichi, T., Inamoto, E., Toyonaga, H., and Mori, H. (2005) *DNA Res.* **12**, 291–299
33. Baykov, A. A., Evtushenko, O. A., and Awaeva, S. M. (1988) *Anal. Biochem.* **171**, 266–270
34. Proudfoot, M., Kuznetsova, E., Brown, G., Rao, N. N., Kitagawa, M., Mori, H., Savchenko, A., and Yakunin, A. F. (2004) *J. Biol. Chem.* **279**, 54687–54694
35. Kimber, M. S., Vallee, F., Houston, S., Necakov, A., Skarina, T., Evdokimova, E., Beasley, S., Christendat, D., Savchenko, A., Arrowsmith, C. H., Vedadi, M., Gerstein, M., and Edwards, A. M. (2003) *Proteins* **51**, 562–568
36. Rosenbaum, G., Alkire, R. W., Evans, G., Rotella, F. J., Lazarski, K., Zhang, R. G., Ginell, S. L., Duke, N., Naday, I., Lazarz, J., Molitsky, M. J., Keefe, L., Gonczy, J., Rock, L., Sanishvili, R., Walsh, M. A., Westbrook, E., and Joachimiak, A. (2006) *J. Synchrotron Radiat.* **13**, 30–45
37. Otwinowski, Z., and Minor, W. (1997) *Methods Enzymol.* **276**, 307–326
38. Terwilliger, T. C., and Berendzen, J. (1999) *Acta Crystallogr. Sect. D Biol. Crystallogr.* **55**, 849–861
39. Terwilliger, T. C. (2000) *Acta Crystallogr. Sect. D Biol. Crystallogr.* **56**, 965–972
40. Terwilliger, T. C. (2003) *Acta Crystallogr. Sect. D Biol. Crystallogr.* **59**, 38–44
41. Vagin, A., and Teplyakov, A. (1997) *J. Appl. Crystallogr.* **30**, 1022–1025
42. McCoy, A. J., Grosse-Kunstleve, R. W., Storoni, L. C., and Read, R. J. (2005) *Acta Crystallogr. Sect. D Biol. Crystallogr.* **61**, 458–464
43. Emsley, P., and Cowtan, K. (2004) *Acta Crystallogr. Sect. D Biol. Crystallogr.* **60**, 2126–2132
44. Murshudov, G. N., Vagin, A. A., and Dodson, E. J. (1997) *Acta Crystallogr. Sect. D Biol. Crystallogr.* **53**, 240–255
45. Collaborative Computational Project, Number 4 (1994) *Acta Crystallogr. Sect. D Biol. Crystallogr.* **50**, 760–763
46. Movahedzadeh, F., Rison, S. C., Wheeler, P. R., Kendall, S. L., Larson, T. J., and Stoker, N. G. (2004) *Microbiology* **150**, 3499–3505
47. Rittmann, D., Schaffer, S., Wendisch, V. F., and Sahm, H. (2003) *Arch. Microbiol.* **180**, 285–292
48. Ke, H., Thorpe, C. M., Seaton, B. A., Marcus, F., and Lipscomb, W. N. (1989) *Proc. Natl. Acad. Sci. U. S. A.* **86**, 1475–1479
49. Marcus, F., Rittenhouse, J., Chatterjee, T., and Hosey, M. M. (1982) *Methods Enzymol.* **90**, 352–357
50. Hines, J. K., Fromm, H. J., and Honzatko, R. B. (2007) *J. Biol. Chem.* **282**, 11696–11704
51. Albert, A., Yenush, L., Gil-Mascarell, M. R., Rodriguez, P. L., Patel, S., Martinez-Ripoll, M., Blundell, T. L., and Serrano, R. (2000) *J. Mol. Biol.* **295**, 927–938
52. McAllister, G., Whiting, P., Hammond, E. A., Knowles, M. R., Atack, J. R., Bailey, F. J., Maigetter, R., and Ragan, C. I. (1992) *Biochem. J.* **284**, 749–754
53. Inhorn, R. C., and Majerus, P. W. (1988) *J. Biol. Chem.* **263**, 14559–14565
54. Johnson, K. A., Chen, L., Yang, H., Roberts, M. F., and Stec, B. (2001) *Biochemistry* **40**, 618–630
55. Zhang, Y., Liang, J. Y., and Lipscomb, W. N. (1993) *Biochem. Biophys. Res. Commun.* **190**, 1080–1083
56. Patel, S., Yenush, L., Rodriguez, P. L., Serrano, R., and Blundell, T. L. (2002) *J. Mol. Biol.* **315**, 677–685
57. Leech, A. P., Baker, G. R., Shute, J. K., Cohen, M. A., and Gani, D. (1993) *Eur. J. Biochem.* **212**, 693–704
58. Pollack, S. J., Atack, J. R., Knowles, M. R., McAllister, G., Ragan, C. I., Baker, R., Fletcher, S. R., Iversen, L. L., and Broughton, H. B. (1994) *Proc. Natl. Acad. Sci. U. S. A.* **91**, 5766–5770
59. Bone, R., Springer, J. P., and Atack, J. R. (1992) *Proc. Natl. Acad. Sci. U. S. A.* **89**, 10031–10035
60. Bone, R., Frank, L., Springer, J. P., and Atack, J. R. (1994) *Biochemistry* **33**, 9468–9476
61. Kuznetsova, E., Proudfoot, M., Gonzalez, C. F., Brown, G., Omelchenko, M. V., Borozan, I., Carmel, L., Wolf, Y. I., Mori, H., Savchenko, A. V., Arrowsmith, C. H., Koonin, E. V., Edwards, A. M., and Yakunin, A. F. (2006) *J. Biol. Chem.* **281**, 36149–36161